Structure and Dynamics of the Solvated Electron in Alcohols from Resonance Raman Spectroscopy

Christina M. Stuart, Michael J. Tauber,*,‡ and Richard A. Mathies*

Department of Chemistry, University of California, Berkeley, California 94720

Received: December 2, 2006; In Final Form: June 14, 2007

Resonance Raman (RR) spectroscopy is used to probe the structure and excited-state dynamics of the solvated electron in the primary liquid alcohols methanol (MeOH), ethanol (EtOH), *n*-propanol (*n*-PrOH), and *n*-butanol (*n*-BuOH). The strong resonance enhancements ($\geq 10^4$ relative to pure solvent) of the libration, CO stretch, COH bend, CH_3 bend, CH_2 bend, and OH stretch reveal significant Franck−Condon coupling of the intermolecular and intramolecular vibrational modes of the solvent to the electronic excitation of the solvated electron. All enhanced bands are fully accounted for by a model of the solvated electron that is comprised of several nearby solvent molecules that are only perturbed by the presence of the electron; no new molecular species are required to explain our data. The 340 cm^{-1} downshift observed for the OH stretch frequency of e^-(MeOH), relative to pure solvent, strongly suggests that the methanol molecules in the first solvent shell have the hydroxyl group directed linearly toward the excess electron density. The smaller downshifts observed for e^-(EtOH), e^-(*n*-PrOH), and e^-(*n*-BuOH) are explained in terms of a OH group that is bent 28−40° from linear. The Raman cross sections and absorption spectra are modeled, lending quantitative support for the inhomogeneous origin of the broad absorption spectra, the necessity of OH local motion in all enhanced Raman modes of the alcohols, and the dominant librational response of the solvent upon photoexcitation of the electron.

1. Introduction

Knowledge of the solvation structure and dynamics of ions in solution is crucial for understanding fundamental processes in chemistry and biology, such as electron transfer and the transport of ions in channels.[1,2] Solvent−solute systems that have long been the focus of both experimental and theoretical studies are the solvated electron in water and other polar liquids. The most extensive pictures of the solvent structure in the vicinity of the solvated electron have been provided by simulations.[3−6] In general, experimental structural insights have been far more difficult to obtain, but data from electron spin resonance measurements have led to models of the electron in aqueous and other glasses.[7−10] More recently, vibrational spectroscopy has provided a new window on the solvent structure in the liquid phase.[11−16] Despite the recent progress, important questions persist, such as the number of nearest neighbors to the electron in the liquid phase and the extent to which each solvent molecule is perturbed by the nearby charge. These questions are, in fact, the fundamental questions that underlie debates between "cavity models" and "molecular anion cluster models" of the solvated electron.[17,18] Additionally, the alternative proposal that the solvated electron is comprised of novel molecular species rather than perturbed solvent molecules is a point of view that persists.[19−21] Separate from questions of structure, fundamental questions about the solvated electron dynamics such as the excited-state lifetimes, rates of solvation on the ground- and excited-state potential energy surfaces, the nature of the non-adiabatic electronic relaxation, and the optical dephasing time have only begun to find answers. The most progress has been made for the hydrated electron, which has benefited from a suite of studies, most notably, femtosecond transient absorption spectroscopy,[22,23] three-pulse photon echo techniques,[24] molecular dynamics simulations,[25−28] resonance Raman,[11−16] and fluorescence spectroscopy.[12]

We have recently turned our attention to resonance Raman studies of electrons solvated in the primary alcohols, in part, to test structural and dynamical insights determined from our studies of solvated electrons in water.[12,13,15] Relative to water, the larger size of the alcohols and the reduced hydrogen bond valency leads to fewer solvent molecules in the first solvation shell around most ionic solutes.[29] Specifically for the solvated electron, electron spin echo envelope modulation (ESEEM) studies of electrons solvated in glassy methanol suggest four molecules in the first solvation shell, whereas electrons in glassy water have six.[7,9] In contrast to the bond-oriented structures found for e^-(MeOH) and e^-(H_2O), the ESEEM studies of solvated electrons in ethanol yield a solvent shell consisting of four molecules that are dipole-oriented toward the electron.[10] It should be noted that, subsequently, important aspects of the ESEEM studies were questioned, as described recently.[30] Interestingly, MD simulations of e^-(MeOH) also suggest bond-oriented solvent molecules in the first solvation shell but show no difference in coordination number for methanol relative to that for water.[4,31,32] To date, experimental evidence on the solvated electron in the liquid alcohols, such as coordination number and orientation in the first solvent shell, is lacking.

From the dynamics standpoint, alcohols are well-known to differ considerably from water. For example, the amplitude of the ultrafast inertial response is thought to be much less

* To whom correspondence should be addressed. E-mail: rich@zinc.cchem.berkeley.edu. Phone: (510) 642-4192. Fax: (510) 642-3599 (R.A.M.); E-mail: mtauber@ucsd.edu. Phone: (858) 534-7334. Fax: (858) 534-4864.

‡ Current Address: Department of Chemistry and Biochemistry, University of California, San Diego, La Jolla, California 92093.

10.1021/jp068283q CCC: $37.00
Published on Web 08/04/2007

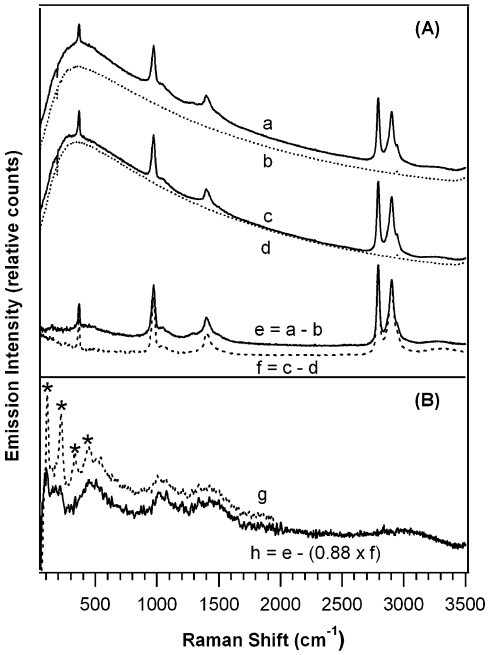

Figure 1. Example of the baseline and background subtraction procedure used to obtain the resonance Raman (RR) spectra of electrons in alcohols. (A) Pump + probe (solid, a) and 229 nm pump-only (dotted, b) spectra of ~5 mM KI in MeOH. Spectral traces c and d were acquired using the same solution after the addition of 80 mM acetone. Direct subtraction of (pump + probe) − (pump only) spectra yields traces e and f, which are, respectively, without and with acetone. Traces a, b and c, d are pairwise offset for clarity. (B) The difference of traces e and f yields the spectrum of the solvated electron in MeOH (h). The scaling factor of 0.88 for trace f was chosen such that the relatively narrow pure-solvent features in the CO and CH stretch regions were neither under- nor over-subtracted. Trace g was obtained using (pump + probe) − (pump-only) − (probe only) − (background only), a method that yields a composite emission spectrum with features from both I_2^-, indicated with asterisks, and the solvated electron. The probe wavelength was 683 nm.

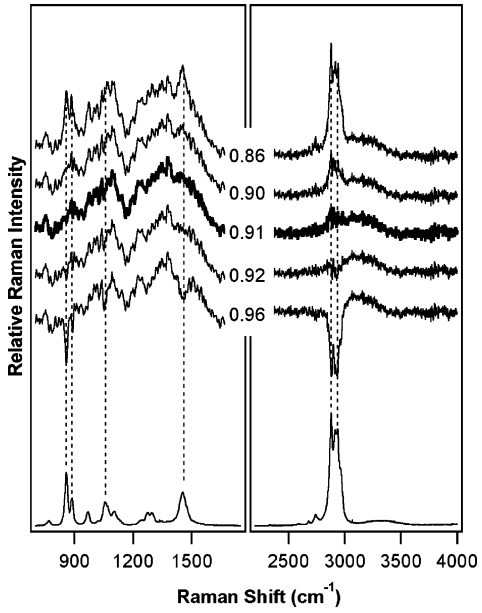

Figure 2. Comparison of the difference spectra obtained by scaled subtraction of spectra acquired without and with acetone for solvated electrons in *n*-propanol. Each trace is labeled with the scaling factors used and shows the over- or under-subtraction of the relatively narrow solvent peaks. The ideal subtraction parameter of 0.91 (bold spectrum) shows complete removal of the sharp solvent peaks and depends on several factors, including electron concentration, jet thickness, and self-absorption effects.

significant for alcohols.[33,34] The response measured by dielectric spectroscopy to nearly 100 GHz shows at least three time scales for relaxation in the alcohols, whereas water has two time scales.[35] Experiments with a ~35 fs time resolution were required to observe the inertial response and strong isotope effect of the fastest response in $e^-(H_2O)$ and $e^-(D_2O)$, a result that was consistent with a 1.4-fold greater fluorescence quantum yield of electrons in D_2O versus that in H_2O, and strong enhancement of the water librational modes in the RR spectra.[12] While transient absorption experiments have contributed substantially to the current understanding of the dynamics of electron−alcohol systems,[36−38] experiments employing a time resolution of <50 fs necessary to observe isotope effects and the inertial response have not yet been performed. Moreover, neither photon echo experiments nor quantitative analysis of the resonance Raman spectra have been performed on electron−alcohol systems, as have been done for the hydrated electron.[13,24] MD simulations and experimental studies have both aimed to find the excited-state lifetime (or rate of nonadiabatic transition) for electrons in alcohols; however, these lifetimes remain uncertain. One MD study reported an excited-state lifetime for e^-(MeOH) that was 3 times longer than the lifetime of $e^-(H_2O)$.[27] More recently, a different simulation reported <100 fs excited-state lifetimes for both e^-(MeOH) and $e^-(H_2O)$.[39] Given the challenge of these calculations and the dearth of ultrafast results, the need for additional information on the excited-state dynamics of the electron in alcohols is evident.

We report here the quantitative analysis of the resonance Raman (RR) spectra of electrons solvated in primary alcohols, which follows our initial account.[40] RR is an ideal technique for probing the Franck−Condon coupling of an electronic excitation to the vibrations of a chromophore and yields mode-specific information on the ultrafast intramolecular and solvation dynamics following electronic excitation.[41] We have quantitatively analyzed the resonance Raman spectra of electrons solvated in primary alcohols including methanol, ethanol, *n*-propanol, and *n*-butanol to investigate solvent structure in the immediate vicinity of the ground-state electron. The resonance Raman frequencies provide new data on the structures of the solvated electron in the liquid state. The analysis of the Raman cross sections and absorption spectra reveals (1) significant Franck−Condon coupling to at least five vibrational modes for each alcohol, (2) the particular importance of the librational mode in the excited-state dynamics after photoexcitation, and (3) the dominant contribution of inhomogeneous broadening to the solvated electron absorption spectra.

2. Materials and Methods

2.1. Generation of Electron and Experimental Overview. Solvated electrons were generated in alcohols by UV excitation of the charge-transfer-to-solvent (CTTS) band of iodide.[42] Solutions of potassium iodide (3.0−12.0 mM, EM Science) were prepared in a series of linear alcohols, methanol (EM Science, Optima Grade), ethanol, *n*-propanol and *n*-butanol (Aldrich), and their fully deuterated or hydroxyl-deuterated analogues (Aldrich and Cambridge Isotopes Labs, 99% purity). A 20 ns delay between the generation of electrons and the arrival of the resonant probe ensured that the electrons were equilibrated in their ground state when probed. Experiments with electrons present were alternated with identical runs where 80 mM acetone (Aldrich) was added to scavenge the electron (see Data Analysis). The near-diffusion-limited rate of reaction of the

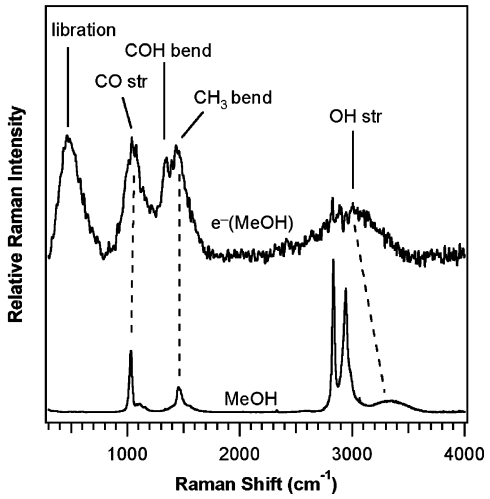

Figure 3. Comparison of the RR spectrum of the solvated electron in methanol, with an off-resonance spectrum of pure solvent. The probe wavelength was 683 nm.

electron with acetone[43] allowed removal of the electrons within the 20 ns pump−probe delay. The solutions were photolyzed and probed as they flowed down a gravity-driven wire-guided film of ~100 μm thickness. Solutions were recirculated with a peristaltic pump[44] and replaced every 50 min to avoid buildup of side products. All reagents were used as received.

Solvated electron concentrations were determined by measuring the change in probe transmission through the liquid film as a result of the pump pulse, together with the known molar extinction coefficients at the probe wavelength of the electron solvated in alcohols[45,46] and the known diagonal path length of the film (~100 μm). The concentration of the electrons averaged across the film ranged from 0.16 to 0.30 mM when photolyzing a 3 mM potassium iodide solution with 218 nm light.

2.2. Optical System. The experimental setup consisted of a 20 Hz Nd:YAG laser (Quanta Ray DCR-2A, 8 ns pulse width) equipped with crystals for generating second and fourth harmonics. The 1064, 532, and 266 nm beams were directed collinearly into a 0.87 m Raman shifter filled with either 100 psi of H_2 or 80 psi of D_2. The output of the shifter was dispersed using a Pellin−Broca prism to isolate the pump and the probe beams. The second anti-Stokes beam from 266 nm yielded the pump pulse at 218 or 229 nm (1.5−2.5 mW). The probe pulse was either 532 nm or the Stokes-shifted lines at 632, 683, or 780 nm (2.0 mW). The pump and probe beams were made collinear with a dichroic beam splitter and directed at the sample in a 45° backscattering geometry. Both beams were cylindrically focused at the sample plane, with typical dimensions of 150 μm × 1 mm for the probe and 300 μm × 3 mm for the pump. The larger dimensions of the pump pulse ensured that the entire probed region contained a significant concentration of electrons.

The emission from the sample was collected by a Mitutoyo M-Plan NIR objective (NA = 0.26, f.l. 20 mm) and focused on the entrance slit of a SPEX 500M spectrograph equipped with a 300 g/mm grating.[15] The dispersed light (resolution = 21 cm^{-1} at 800 nm) was then imaged on a liquid-nitrogen-cooled front-illuminated open-electrode CCD (Roper Scientific LN/CCD 1024-E/OP/1). Rayleigh scattering was rejected with a Kaiser Optical SuperPlus Notch filter (532, 683, or 780 nm) or long-pass filter (RG645 for 632 nm). All spectra were corrected for the instrument response and self-absorption effects. Self-absorption corrections were determined by comparison of the solvent peak intensities in the presence and absence of the electron.

2.3. Data Analysis. The pump + probe Raman spectrum of dilute potassium iodide in methanol is shown in Figure 1A. Subtraction of the pump-only (b) from the pump + probe (a) spectrum removed the stray laser lines and the fluorescence background due to the pump pulse and yields trace e, which has contributions from bulk methanol, the solvated electron, and the intermediate I_2^-. After the addition of 80 mM acetone, pump + probe and pump-only Raman spectra were again collected (c and d, respectively). The difference of these two spectra yields f, which has contributions from bulk methanol and I_2^-. The spectrum of e^-(MeOH) was obtained by a carefully scaled subtraction (see below) of trace f from trace e, which yields the spectrum of the solvated electron, h (Figure 1B).

Figure 1B compares the result of the subtraction scheme outlined above with an earlier procedure used to obtain solvated electron spectra using I^- as the electron source in aqueous solution.[13] Trace g was obtained using the earlier subtraction procedure, (pump + probe − pump-only) − (probe-only background), and reveals a low-frequency vibrational progression (indicated with asterisks) that is not apparent in spectrum h. The subtraction procedure utilizing acetone as a scavenger, reported earlier[40] and described in detail above, is evidently necessary when using KI as the electron source to remove Raman scattering and fluorescence from an intermediate species that is resonant with the probe[47] and to ensure all vibrational and fluorescence features are due entirely to the solvated electron.

Special care in the subtraction of spectra with and without acetone was necessary to determine which vibrational bands of the solvent are resonantly enhanced. We illustrate a range of subtraction parameters for e^-(*n*-PrOH) (Figure 2). The traces are obtained using subtraction parameters ranging from 0.86 to 0.96. Sharp peaks in the 700−1700 cm^{-1} and in the 2700−3100 cm^{-1} regions appear as positive features with under-subtraction and as negative features with over-subtraction. The fact that the over- or under-subtracted features (1) have a bandwidth that is indistinguishable from the corresponding bands of the pure solvent and (2) maintain the same intensity ratios relative to the pure solvent support our conclusion that these bands are due to the pure solvent and are not resonantly enhanced bands of the solvated electron. The optimal subtraction parameter was always less than 1, as expected since it corrects for the attenuation of solvent Raman scattering due to absorption by the electrons. The exact value of the parameter therefore depends mostly upon the concentration of electrons. For all data sets, the parameter was systematically chosen to minimize the appearance of any positive or negative pure solvent features across the spectral window and was found to vary less than 10% from run to run. The subtraction parameter also allows for cancellation of minor fluctuations in average laser power (<5%) that may occur during interleaved pump + probe, pump-only, and probe-only spectra.

2.4. Resonance Raman Calculations. Absolute Raman cross sections of the solvated electron vibrations were determined using the following equation[41]

$$\sigma_{e^-} = \frac{8\pi}{3}\frac{(1+2\rho)}{(1+\rho)}\left(\frac{\partial\sigma_{e^-}}{\partial\Omega}\right)_{||+\perp} \qquad (1)$$

where $\partial\sigma_{e^-}/\partial\Omega$ is the differential cross section for the solvated electron, obtained by comparing the integrated areas of the solvated electron bands to methanol's symmetric CH_3 stretch band at 2837 cm^{-1} ($\partial\sigma_{std}/\partial\Omega = 8.30 \times 10^{-14}$ Å^2/molecule/

TABLE 1: Raman Vibrational Parameters and Cross Sections for the Solvated Electron in Primary Alcohols

e^-(MeOH)	520 cm^{-1}		1060 cm^{-1}		1360 cm^{-1}		1470 cm^{-1}		2990 cm^{-1}	
	fwhm (cm^{-1})	σ_R ($\times 10^9$ Å^2)	fwhm (cm^{-1})	σ_R ($\times 10^9$ Å^2)	fwhm (cm^{-1})	σ_R ($\times 10^9$ Å^2)	fwhm (cm^{-1})	σ_R ($\times 10^9$ Å^2)	fwhm (cm^{-1})	σ_R ($\times 10^9$ Å^2)
532 nm	233	11.8	225	8.9	145	2.9	175[a]	4.2	548	8.9
632 nm	203	14.3	225	10.3	133	4.3	175[a]	5.5	483	6.9
683 nm	213	11.0	217	8.2	175[a]	3.7	175[a]	5	554	5.3
780 nm	176	2.2	163	1.4	175[a]	1	175[a]	1.1		

e^-(EtOH)	480 cm^{-1}		1080 cm^{-1}		1265 cm^{-1}		1370 cm^{-1}		1470 cm^{-1}		3040 cm^{-1}	
532 nm	225	11.6	145	4.9	111	2.9	109	1.8	180	3.8	363	3.1
632 nm	190	12.7	177	5.8	101	2.7	108	2.2	206	5.6	467	3.9
683 nm	205	12.7	157	5.3	107	2.9	113	2.3	193	4.7	428	4.3
780 nm	176	2.9	131	1.1	109	0.7	123	0.7	189	1.5		

e^-(*n*-PrOH)	460 cm^{-1}		1070 cm^{-1}		1260 cm^{-1}		1355 cm^{-1}		1470 cm^{-1}		3060 cm^{-1}	
532 nm	189	12.9	246	5.9	100[a]	1.8	100[a]	1.9	210	4.7	472	5.2
632 nm	195	16.2	307	6.3	100[a]	1.7	100[a]	2.1	224	5.6	398	3
683 nm	208	13.5	270	5.7	100[a]	1.6	103	2.3	183	4	447	3.8
780 nm	173	2.6	218	0.9	100[a]	0.4	100[a]	0.5	197	1.3		

[a] The widths have been held constant during fit iterations.

steradian at 488 nm excitation).[48] The symmetric CH_3 stretch band of the respective solvent was used as the internal standard for all experiments, except for the 780 nm experiments where the CO stretch was used. The depolarization ratios, ρ, for all bands of the solvated electron in methanol were measured and found to be 1/3, as expected for a resonant transition.

Raman excitation profiles (REPs) were determined from calculations of a nonstationary wavepacket $|i(t)\rangle$ that propagates on a multidimensional excited-state surface. The overlap of $|i(t)\rangle$ with the stationary initial state $|i\rangle$ determines the absorption cross section, and the overlap with the final stationary vibrational state $|f\rangle$ yields the RR cross sections. The time-dependent overlaps depend parametrically upon a set of displacements (Δ's) between the ground and excited states along the normal coordinates that are coupled to the electronic transition. The absorption, σ_A, and Raman, σ_R, cross sections are then obtained from the following Fourier transforms[41]

$$\sigma_A = \frac{4\pi E_L e^2 M^2}{6\hbar c n(\theta\sqrt{2\pi})} \int_0^\infty dE \exp\left[\frac{-(E-E_0)^2}{2\theta^2}\right] \times \int_{-\infty}^{\infty} dt \langle i|i(t)\rangle e^{-\Gamma_G t/\hbar} e^{i(E_L+\epsilon_i)t/\hbar} \quad (2)$$

$$\sigma_R = \frac{8\pi E_s^3 E_L e^4 M^4}{9\hbar c^4(\theta\sqrt{2\pi})} \int_0^\infty dE \exp\left[\frac{-(E-E_0)^2}{2\theta^2}\right] \times \left| \int_0^\infty dt \langle f|i(t)\rangle e^{-\Gamma_G t/\hbar} e^{i(E_L+\epsilon_i)t/\hbar} \right|^2 \quad (3)$$

where E_L and E_S refer to the frequency of the laser and scattered radiation in wavenumbers, M is the transition moment, E_0 is the zero−zero energy, ϵ_i is the vibrational energy of eigenstate i, Γ_G is the Gaussian homogeneous broadening, and θ is the Gaussian inhomogeneous broadening. A Gaussian was chosen to model the broadening because the red edge of the absorption spectra is known to fit well to this band shape.[24,49,50]

Raman intensity calculations were carried out to model the experimental data by iteratively adjusting θ and E_0 for a selected Γ_G to reproduce the low-energy absorption spectrum and then adjusting the dimensionless displacements (Δ's) to fit the experimental RR cross sections. Only the red edge of the absorption spectrum was used to constrain the calculations since the blue edge is due to transitions from the ground state to higher electronic or continuum states.[49] The Δ's obtained from these calculations can be used to yield the actual excited-state Cartesian displacement along a specific internal coordinate from the following equation[41]

$$\delta_i = 5.8065 \sum_j A_{ji} \omega_j^{-1/2} \Delta_j \quad (4)$$

where δ_i is the ground-state to excited-state geometry change along internal coordinate i with units of angstroms for bond length changes and degrees for changes in angle; A_{ji} is an element of the matrix relating the normal coordinates, j, to the internal coordinate basis set, i; ω_j is the frequency of the normal mode; and Δ_j is the dimensionless displacement along a normal coordinate j, which is obtained from our REP calculations. The A_{ji} matrix elements used in the electron−alcohol systems are assumed to be the same as those for the monomeric solvent and were determined from an optimization and frequency calculation using Gaussian 03.[51] A basis set of normal modes was generated, and the displacements in Cartesian coordinates were converted to the internal coordinate basis set.

3. Results

3.1. Resonance Raman Features of the Solvated Electron. The resonance Raman spectrum of the solvated electron in methanol and the off-resonance spectrum of methanol probed at 683 nm are presented in Figure 3. RR spectra of solvated electrons in submillimolar concentrations exhibit remarkable enhancements ($\sim 10^4$) relative to the cross sections of the pure solvent[48] for the following normal modes, librations ($\sim$520 cm^{-1}), CO stretch (1060 cm^{-1}), COH bend (1360 cm^{-1}), CH_3 bend (1470 cm^{-1}), and the OH stretch (2990 cm^{-1}). Surprisingly, we find no evidence for enhancement in the CH stretch region. The Raman cross sections for each of the enhanced modes at each excitation wavelength are summarized in Table 1.

Comparison of the e^-(alcohol) RR spectra with their respective pure solvent Raman spectra demonstrates that, in addition to resonance enhancements, there are also frequency shifts. Most noticeable is the $\sim$260−340 cm^{-1} frequency downshift of the OH stretch relative to the pure solvent. Other examples are the COH bend ($\sim$1360 cm^{-1}) and one libration (520 cm^{-1}) of e^-(MeOH), which are respectively downshifted by $\sim$20 and

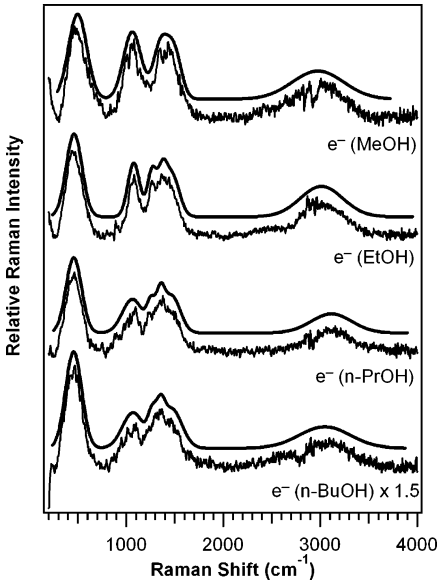

Figure 4. RR spectra of the solvated electron in methanol, ethanol, *n*-propanol, and *n*-butanol with 683 nm excitation. All spectra are normalized for probe energy and electron concentration. Spectra are also corrected for instrument response and self-absorption by the electrons. The spectrum of e^-(*n*-BuOH) is multiplied by a factor of 1.5 for display. A simulated spectrum resulting from a sum of Gaussian band fits is presented above each spectrum, and the optimized peak positions are column headers in Table 1. Portions of the data are reproduced from ref 40.

$\sim$140 cm^{-1} relative to the pure solvent. The frequency shifts of the libration and COH bend are not visible in Figure 3 because these modes have low Raman intensity for the pure solvents; however, the downshift is determined by comparison with known IR spectra.[52] Similar shifts are observed for all electron−alcohol systems studied.

3.2. Comparison of Solvated Electrons in Linear Alcohols. Vibrational spectra of the electron solvated in the series of linear alcohols from methanol to *n*-butanol are presented in Figure 4. In general, the resonance Raman spectra of the solvated electron in ethanol and longer chain alcohols are very similar to the spectrum of e^-(MeOH). All systems show similar enhancements for the libration, CO stretch, COH bend, CH_3 bend, and OH stretch. Spectra of e^-(EtOH), e^-(*n*-PrOH), and e^-(*n*-BuOH) show additional Raman intensity in the CH_2 bending band ($\sim$1470 cm^{-1}). The lengthened alkyl chain changes the Raman intensities but does not qualitatively affect which vibrational modes couple to the electronic transition. The spectra of e^-(*n*-PrOH) and e^-(*n*-BuOH), for example, show virtually indistinguishable vibrational profiles, and only the overall Raman intensities are lower for the e^-(*n*-BuOH) as compared to those for e^-(*n*-PrOH).

3.3. Investigation of the OH Stretch Frequency. Figure 5A illustrates the OH stretch region of the solvated electron in the series of alcohols. The frequency of the solvated electron OH stretch is downshifted relative to the pure solvent and is found at 2990 cm^{-1} for e^-(MeOH), 3040 cm^{-1} for e^-(EtOH), 3060 cm^{-1} for e^-(*n*-PrOH), and 3060 cm^{-1} for e^-(*n*-BuOH). By comparison, the pure solvents show maximum Raman intensity at a nearly constant position for all alcohols, 3330 cm^{-1} for MeOH, 3340 cm^{-1} for EtOH, 3320 cm^{-1} for *n*-PrOH, and 3330 cm^{-1} for *n*-BuOH (Figure 5B). The frequency downshift for the electron−alcohol systems relative to the pure solvent plateaus as the carbon chain lengthens, as shown in Figure 5C.

3.4. Raman Scattering of Skeletal Vibrations. Spectra of the skeletal vibrations of the electron solvated in isotopologues

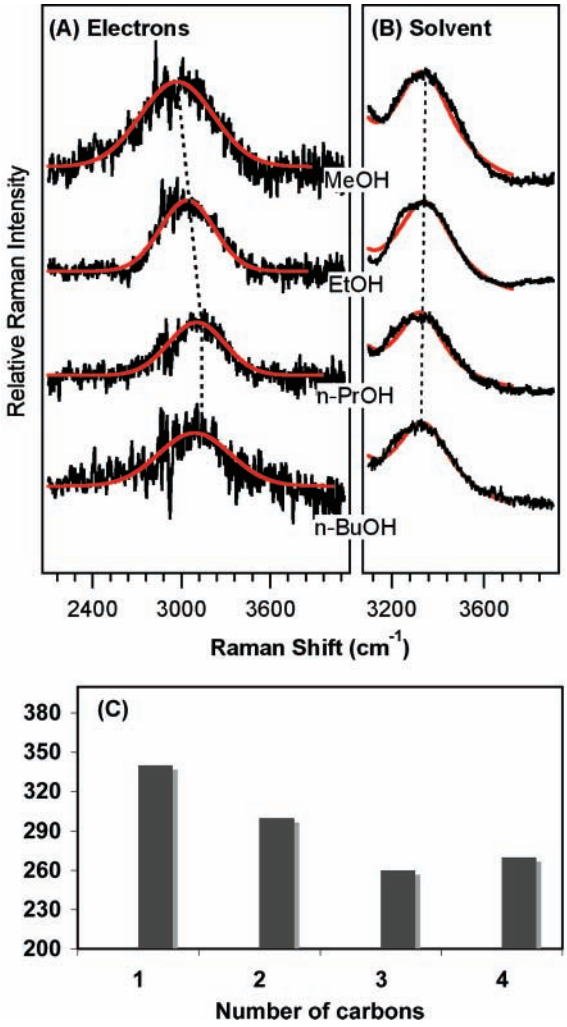

Figure 5. Comparison of the OH stretch frequency for solvated electrons with the respective OH stretch frequency for the pure solvent. (A) The OH stretch region of the solvated electron in each of the primary alcohols is fit to a single Gaussian, with peak frequencies listed in Table 1. RR spectra are normalized for probe power and electron concentration. The e^-(*n*-BuOH) spectrum is multiplied by a factor of 1.5 for display. (B) The OH stretch frequencies for the pure solvent with the peak fit shown. Maxima of the OH stretch were determined from the peak fits. (C) The lower plot displays the shift of OH stretch frequency relative to the pure solvent as a function of alkyl chain length.

of methanol are presented in Figure 6. A reasonable fit to the CO stretch, COH (COD) bend, and CH_3 (CD_3) bend bands in this region are obtained with a sum of three or four Gaussian bands. In some cases, the fits are broadened due to merged bands; therefore, we do not report the widths for all isotopologues studied. Four bands were necessary for all solvents except CH_3OH because the CH_3/CD_3 rock becomes spectrally distinct from the CO stretch upon partial or full deuteration of the solvent. Assignments of the vibrational modes of e^-(MeOH) are based on the observed isotopic shifts as well as prior vibrational studies of pure methanol.[53,54] The band at $\sim$1360 cm^{-1} is assigned as the COH bend based upon its shift to $\sim$ 890 cm^{-1} when the hydroxyl group is deuterated. Similarly, the $\sim$1470 cm^{-1} (1100 cm^{-1}) band is clearly assigned as a CH_3 (CD_3) bending mode. The remaining band in this region is assigned as the CO stretch ($\sim$1060 cm^{-1}) that shifts only slightly with isotopic substitution. Cross sections of the various modes are determined by integrating each band and comparing with the CO stretch and CH stretches of the pure solvent as internal standards (see Table 1).

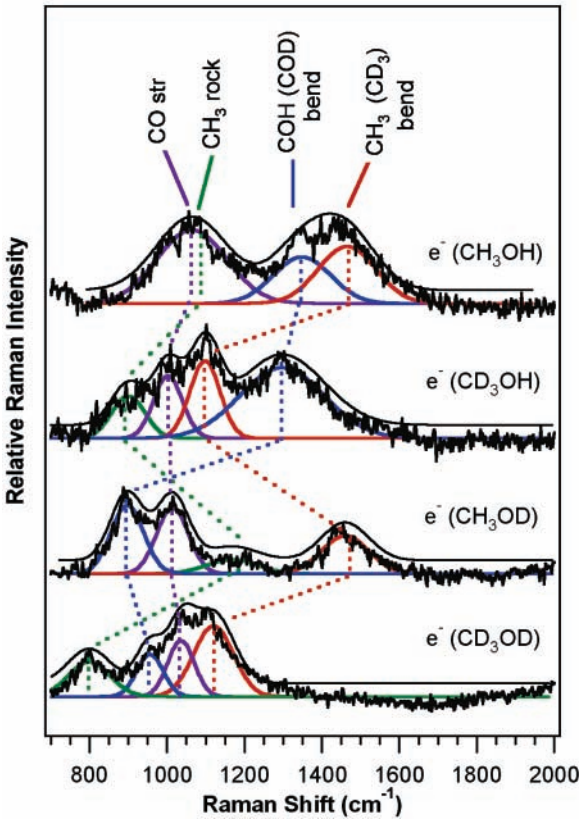

Figure 6. Skeletal Raman scattering from the solvated electron in methanol. Individual Gaussian peak fits are shown, as well as their summation (offset). The parameters used for the fit are listed in Table 1. Modes in common for each solvent are correlated with dashed lines. The probe wavelength was 683 nm. Portions of the data are reproduced from ref 40.

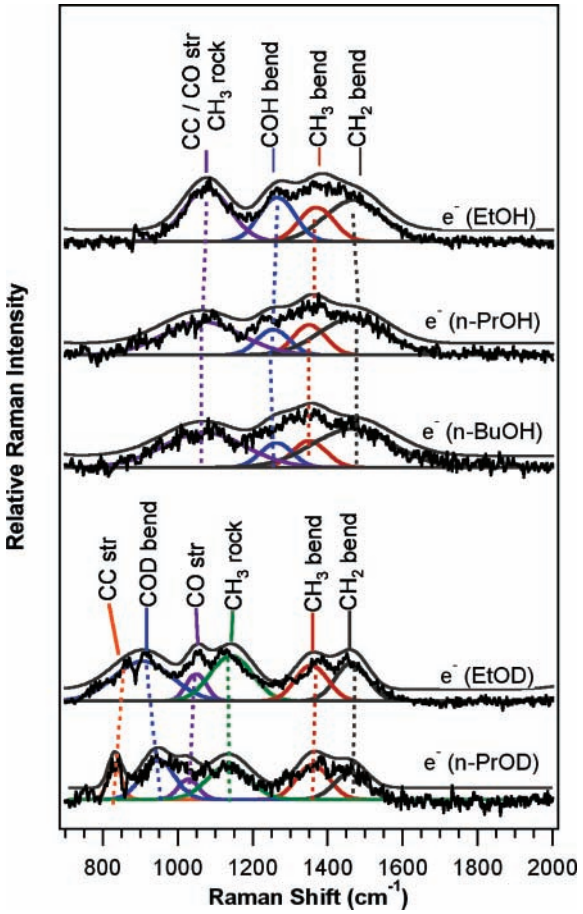

Figure 7. Skeletal Raman scattering from the solvated electron in ethanol, *n*-propanol, and *n*-butanol, and two deuterated isotopologues. Individual Gaussian peak fits are shown, as well as the summation (offset), with peak frequencies for electrons solvated in the fully protiated alcohols listed in Table 1. Modes in common for each solvent are correlated with dashed lines. The probe wavelength was 683 nm.

The skeletal region of the RR spectra of e^-(EtOH), e^-(*n*-PrOH), e^-(*n*-BuOH), and their hydroxyl-deuterated analogues are fit to four or five Gaussian bands (Figure 7). The bands correspond to the CC/CO stretch, COH (COD) bend, CH_3 bend, and CH_2 bend normal modes. Deuteration of the hydroxyl group simultaneously shifts the CH_3 rock to higher frequencies ($\sim$1165 cm^{-1}) as a result of the vibrational coupling between the two modes.[53] Consequently, the deuterated solvents required introduction of an additional band in the fits that takes into account the resolved CH_3 rock. The use of a variety of isotopically labeled solvents allows unambiguous assignment of the COH (COD) bend at 1270 cm^{-1} (910 cm^{-1}) and librations at 480 cm^{-1} (350 cm^{-1}) based on the expected $\sqrt{2}$ shift in frequencies upon deuteration. As expected, the CO stretch ($\sim$1080 cm^{-1}), CH_3 bend ($\sim$1370 cm^{-1}), and CH_2 bend ($\sim$1470 cm^{-1}) are not shifted upon deuteration of the hydroxyl group and are assigned based on their characteristic frequencies. Cross sections of the various modes are determined by integrating each band and comparing with the CO stretch and CH stretches of the pure solvent as internal standards (see Table S2 in Supporting Information).

3.5. Raman Intensity Calculations. Raman intensity calculations were performed to quantify the coupling of the vibrational modes of each solvent with the electronic excitation of the electron. The displacements along five to seven modes for each solvent were optimized to reproduce their respective experimental 683 nm cross sections while simultaneously fitting the respective experimental absorption spectrum of the solvated electron. As a result of the broad featureless absorption spectra, there are multiple parameter sets (Γ_G, Δ, and θ; see rows of Table 2) that produce an equally good match to the red half-width of the experimental absorption spectra and the set of experimental RR cross sections. For example, in the case of e^-(MeOH), each of the four rows of Table 2 comprises a set of parameters that results from initial selection of the homogeneous broadening over a 4-fold range (from 330 to 1330 cm^{-1}). Figure 8 shows nearly identical fits to the absorption spectra of e^-(MeOH) over the full range. The optimized Huang−Rhys factors ($S = \Delta^2/2$) were found to vary by factors of 9−100 in order to maintain the correct Raman cross sections for each normal mode. Figure 9 (plots a−e) shows equally good fits to the observed experimental Raman cross sections for $\Gamma_G = 330$, 670, 1000, and 1330 cm^{-1}. In general, when one selects a larger Γ_G (faster homogeneous dephasing), the corresponding displacements, Δ's, increase to match the measured experimental cross sections, and the inhomogeneous broadening decreases to maintain a good fit to the experimental absorption spectrum. The experimental cross section at 532 nm appears consistently higher than the calculated REPs, which may be attributed to contributions from higher electronic states that are not accounted for in our model. Similar REPs are obtained using a six-mode model for e^-(EtOH) (plots f−k) and e^-(*n*-PrOH) (see Supporting Information, Figure 1S).

One important limit was that homogeneous broadenings needed to be $\leq$1330 cm^{-1} for e^-(MeOH) and e^-(EtOH) because larger values led to poor fits to the well-defined red edge of the absorption spectrum, regardless of the choice of the inhomo-

TABLE 2: Multimode Vibronic Parameters of Electrons in a Series of *n*-Alcohols[a,b]

Multimode Vibronic Parameters of e^-(MeOH)

Γ_G[c]	θ[c]	E_0	S (unitless)					$\Delta E_{1/2}$[d]
			520 cm^{-1}	1060 cm^{-1}	1360 cm^{-1}	1470 cm^{-1}	2990 cm^{-1}	
330	2925	14145	0.010	0.005	0.003	0.003	0.006	2907
670	2840	14075	0.07	0.02	0.01	0.01	0.01	2907
1000	2710	13875	0.26	0.06	0.03	0.02	0.02	2907
1330	2380	13240	0.93	0.21	0.09	0.06	0.05	2890

Multimode Vibronic Parameters of e^-(EtOH)

Γ_G[c]	θ[c]	E_0	S (unitless)						$\Delta E_{1/2}$[d]
			480 cm^{-1}	1080 cm^{-1}	1265 cm^{-1}	1370 cm^{-1}	1470 cm^{-1}	3040 cm^{-1}	
330	2930	12885	0.014	0.004	0.002	0.002	0.003	0.005	2907
670	2855	12815	0.105	0.014	0.007	0.005	0.010	0.010	2907
1000	2715	12575	0.44	0.05	0.02	0.01	0.03	0.02	2907
1330	2350	11575	1.80	0.19	0.08	0.05	0.10	0.04	2907

Multimode Vibronic Parameters of e^-(*n*-PrOH)

Γ_G[c]	θ[c]	E_0	S (unitless)						$\Delta E_{1/2}$[d]
			460 cm^{-1}	1070 cm^{-1}	1260 cm^{-1}	1355 cm^{-1}	1470 cm^{-1}	3060 cm^{-1}	
330	2870	13085	0.024	0.006	0.002	0.003	0.004	0.007	2839
670	2750	12930	0.21	0.026	0.006	0.008	0.012	0.015	2822
1000	2495	12095	1.44	0.15	0.03	0.04	0.06	0.03	2839

[a] All values listed are in wavenumbers, unless otherwise indicated. [b] Raman cross sections were the same for all rows after the deltas were varied to obtain experimental values listed at 683 nm. [c] HWHM listed and adjusted from eqs 1 and 2 using $\Gamma_G(\text{HWHM}) = 2\sqrt{\ln 2}\Gamma_G$ and $\theta(\text{HWHM}) = \sqrt{2\ln 2}\theta$. [d] $\Delta E_{1/2}$ is the calculated low-energy HWHM.

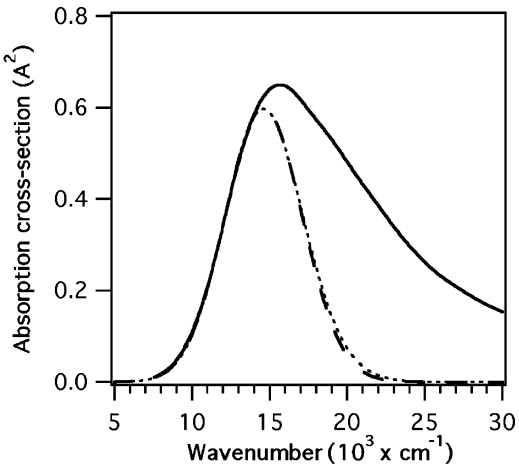

Figure 8. Absorption spectrum of electrons solvated in methanol from experimental data of Jou and Freeman (—).[49] The calculated absorption spectra using a five-mode model with a homogeneous broadening of 330 (dashed line) and 1330 cm^{-1} (dotted line) both yield a good match to the red edge of the experimental absorption spectrum. The blue edge is intentionally not fit in the calculation because the experimental intensity in this region is derived from transitions to higher electronic or continuum states.

geneous broadening input. Additionally, all parameter sets indicate that inhomogeneous broadening outweighs homogeneous broadening. This result contrasts with the dominant homogeneous broadening found for the hydrated electron.[13,24] Similar conclusions were reached for solvated electrons in EtOH and *n*-PrOH, as tabulated in Table 2.

Resonance Raman intensity calculations were also performed for the electron solvated in hydroxyl-deuterated analogues of methanol, ethanol, and *n*-propanol. The calculations were performed with simultaneous fits to the absorption spectra of the electron solvated in the respective protiated alcohol since spectra of electrons solvated in deuterated alcohols are generally unavailable. However, one report that compares $e^-(CH_3OH)$ and $e^-(CD_3OD)$ found the absorption spectra to be nearly indistinguishable.[47] Consistent with this finding and the known similarity of the half-widths of the low-energy wings of $e^-(H_2O)$ and $e^-(D_2O)$,[55] we expect that all deuterated alcohols should have very similar, if not identical, spectra compared with their protiated isotopologues. The parameters used to calculate the absorption spectra (Table S3) and REPs of electrons in deuterated alcohols are presented (Figure S2) in the Supporting Information. With variations of Γ_G over a 4-fold range, the Δ's must vary by factors of 5−30 to obtain the correct calculated cross sections to match experimental data. Good agreement is obtained between the observed and calculated cross sections when the homogeneous broadening parameter is $\leq$1000 cm^{-1}. Again, all of the sets of parameters that yield good fits reveal that inhomogeneous broadening dominates the breadth of the electronic absorption spectra.

4. Discussion

4.1. Structure of the Solvated Electron in Alcohols. Our RR data limit the possible structural models for the solvated electron. The most important point about the spectra of the solvated electron in water, methanol, ethanol, *n*-propanol, and *n*-butanol is the following observation: all bands are well-correlated with corresponding vibrational bands of the pure solvent. The shifts in vibrational frequencies reveal that the hydrogen bond structure of the bulk solvent is perturbed in the presence of the electron; however, we find no evidence for the formation of new molecular species. These conclusions based on our experimental spectra contradict those based on recent calculations, which suggest that the solvated electron can be modeled in water or methanol as a solvated H_3O or CH_3OH_2 radical that dissociates into an electron and H_3O^+ and $CH_3OH_2^+$ cation, respectively.[20,21]

To prevent any misunderstanding of the factual basis of this discrepancy, we go through each observation in detail. Our experimental spectra of $e^-(CH_3OH)$ are free of Raman intensity in the 1650−2400 cm^{-1} spectral window, which is a crucial

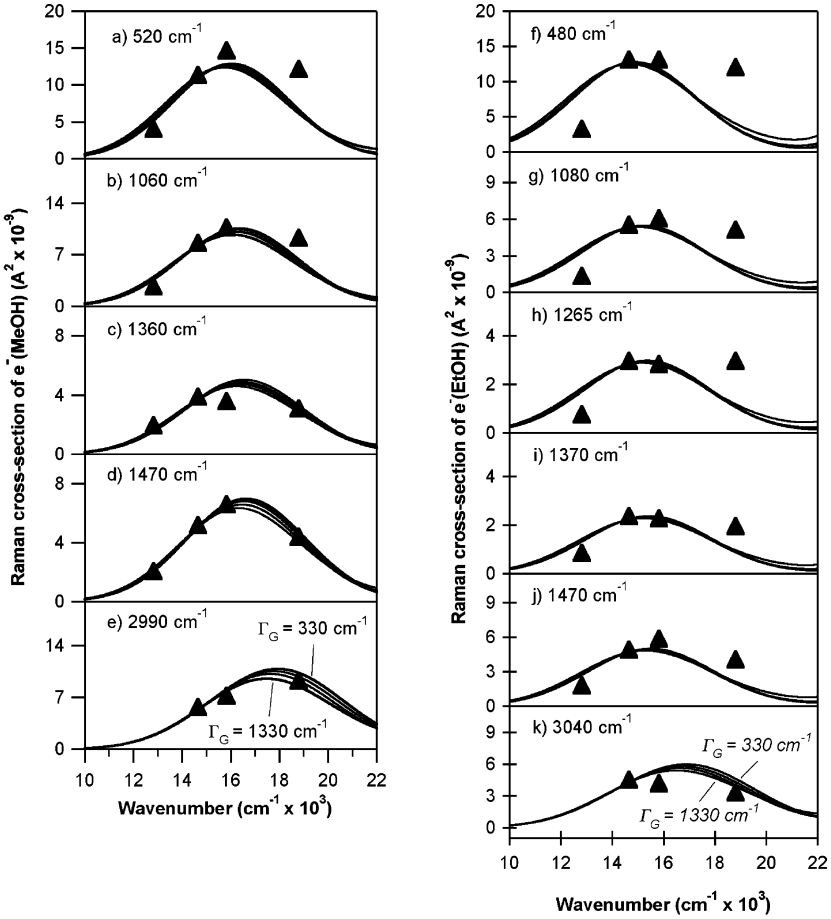

Figure 9. Raman excitation profiles (lines) compared to the experimental cross sections (points) for solvated electrons in CH_3OH (a−e) and the solvated electron in CH_3CH_2OH (f−k). The overlapping traces are for parameter sets ranging from $\Gamma_G = 330-1330$ cm^{-1} for methanol and $\Gamma_G = 330-1330$ cm^{-1} for ethanol. Similar fits are obtained for solvated electrons in *n*-propanol and deuterated solvents (see Figure S1 and S2 in Supporting Information).

region within which vibrational bands of the HOH part of the hypothesized $CH_3OH_2^+$ species are calculated.[21] The calculation shows strong Raman bands peaked at 1650 and 1730 cm^{-1}, which are respectively assigned to the HOH asymmetric stretch and HOH bend of the $CH_3OH_2^+$ species solvated by three methanol solvent molecules.[21] Additionally, a smaller band peaked at 2080 cm^{-1} is calculated and assigned to a HOH symmetric stretch of the same solvated species.[21] Second, there is the absence of calculated CH_3 bend intensity that is prominently peaked in the experimental spectrum at ∼1470 cm^{-1} and was unambiguously assigned from isotope studies.[40] There are also some bands where experimental and calculated spectra show general agreement, such as the enhanced OH stretch and OH torsion (libration). However, in terms of specifically addressing the claim of a $CH_3OH_2^+$ species, these additional bands are not nearly as direct a probe as the HOH bands computed within the 1650−2400 cm^{-1} spectral window that are absent from our spectra. In short, unless the HOH vibrations of the proposed $CH_3OH_2^+$ species become Raman inactive in the larger clusters (which does not appear to be a trend in Figure 4 of Neumann et al.[21]), our data do not support the incorporation of a $CH_3OH_2^+$ species in any model of the solvated electron.

Our data provide information on the nature of the solute−solvent interaction, the solvent orientation, and the magnitude of the Franck−Condon coupling, all of which support a model of the solvated electron that we briefly outline here. Solvation of the electron results in reorientation of multiple solvent molecules in the vicinity of the electron. The RR spectra depend upon Franck−Condon coupling of specific solvent modes to the electronic transition, and we find that only modes with significant contribution from a OH internal coordinate are RR active. Furthermore, an analysis of the OH stretch frequency downshifts indicates that the OH group is bond-oriented toward the electron in the case of methanol but more dipole-oriented in the case of ethanol and longer alcohols. Last, our data suggest that there are significantly fewer solvent alcohol molecules in the first solvent shell relative to the hydrated electron. The evidence behind these conclusions and other aspects of our model of the solvated electron are explored in the following sections.

4.2. Frequency Shifts. Frequency downshifts of hundreds of wavenumbers are observed for the OH stretch and the librations of the alcohols in the presence of the solvated electron. The OH stretch frequency reports on the nature and strength of the electron−alcohol interaction.[40,56−58] In the pure alcohols, the OH stretch frequency occurs at ∼3320−3340 cm^{-1}. The electron solvated in methanol exhibits a remarkable downshift of 340 cm^{-1} relative to pure solvent, and downshifts of 300−260 cm^{-1} are seen for e^-(EtOH), e^-(*n*-PrOH), and e^-(*n*-BuOH). In contrast, Raman studies of halides solvated in the pure alcohols show upshifts for the OH stretching frequency, relative to pure solvent.[59,60] This upshift is also consistent with studies investigating the effect of halides on the Raman spectrum of water.[61,62] It is clear that the electron perturbs the liquid solution in a very different way than the halides. The ideal comparison to our work on the solvated electron would be found in vibrational studies of anionic clusters, for example, $(CH_3OH)_n^-$,

but to our knowledge, only photoelectron studies without vibrational resolution of anionic methanol clusters have been reported thus far.[63]

The downshifted OH stretch frequency, which is unique to the solvated electron system, can be explained from the viewpoint of electrostatics or charge-transfer effects. Electric fields are well-known to shift vibrational frequencies, as has been explored both experimentally and theoretically.[64] The OH stretch frequency depends linearly on the magnitude of the electric field that is parallel to the axis of the vibration (vibrational Stark effect).[64] The parallel electric field E that affects the OH bond strength in the case of the solvated electron can be written approximately as

$$E_{||} = \frac{1}{4\pi\epsilon_o}\frac{q\cos\theta}{r^2} \tag{5}$$

where θ is the angle formed by the OH bond dipole vector relative to the electron−dipole distance vector $\vec{\mathbf{r}}$; r is the distance between the center of the electron charge and the center of the OH dipole, and q is the electron charge. Using this equation and the observed OH frequency downshifts ($\Delta\nu$), we can compute the relative angle θ formed by the electron and OH bond in two e$^-$−alcohol systems (i.e., MeOH and EtOH), assuming a constant distance between the electron and the nearby OH group

$$\Delta\nu \propto \frac{\cos\theta}{r^2} \tag{6}$$

As a point of reference, we assume that solvated electrons in liquid methanol are bond-oriented ($\theta = 0°$), which seems very likely given two facts. First, bond orientation is established for the hydrated electron system at room temperature from RR studies of the mixed isotopologue e$^-$(HDO).[15] Second, the magnitude of the OH frequency downshift for e$^-$(MeOH) substantially exceeds even that of the hydrated electron. Since any angular deviation from a linear electron−HO configuration would diminish the downshift for e$^-$(MeOH), the experimental facts suggest bond orientation characterizes e$^-$(MeOH) in the liquid phase. Using eq 6 and the 340 cm^{-1} downshift of e$^-$(MeOH) as a reference ($\theta = 0°$), a bond angle change of 28° would account for the 300 cm^{-1} downshift for e$^-$(EtOH) and 40° for the 260−270 cm^{-1} downshifts for e$^-$(*n*-PrOH) and e$^-$(*n*-BuOH). Thus, the electrostatic analysis suggests that the hydroxyl group of CH_3OH is largely directed toward the center of the excess electron charge distribution, while the solvent molecules approach dipole orientation in the case of ethanol and longer alcohols (the molecular dipole in alcohols approximately bisects the COH angle). Interestingly, these results for the liquid phase are in nearly quantitative agreement with conclusions based on ESEEM studies of both e$^-$(MeOH) and e$^-$(EtOH) glasses.[9,10]

Another possible hypothesis for the trend in OH stretch frequencies attributes the variation in frequency downshift to changes in the electron−hydrogen distance while assuming the OH bond is linearly directed toward the electron in all alcohols (fixed-bond orientation). The relationship between fractional change in frequency downshift to the fractional change in radius is readily derived from eq 6

$$\frac{\partial(\Delta\nu)}{\Delta\nu} = \frac{-2\partial r}{r_{12}} \tag{7}$$

From the experimental downshifts and eq 7, we would conclude that the electron−hydrogen distance is 7% greater for the solvated electron in ethanol and 12% greater for that in *n*-propanol, both relative to the electron−hydrogen distance of e$^-$(MeOH). The variations in r can be attributed to either steric effects or dielectric properties of each solvent (see Supporting Information). Regardless of the underlying reason for the change in r, the conclusion of an increased radius for e$^-$(EtOH) is inconsistent with ESEEM data that indicate the opposite trend, namely, that the distance between the hydroxyl hydrogen and the electron is 9% smaller in e$^-$(EtOH) than in e$^-$(MeOH).[9,10] For this reason, we prefer the variation in the electron−hydrogen bond angle (at constant distance) as the explanation for our RR downshifts.

A more complete understanding of the electron−solvent interaction must include significant charge-transfer effects.[65] In fact, it is from this point of view that we find an intriguing explanation for the ∼70% greater downshift of the OH stretch observed for the e$^-$(MeOH) relative to that for e$^-$(H_2O). In the charge-transfer model, it is reasonable to postulate that the strength of interaction with any one solvent molecule should scale inversely with the number of molecules present. If the solvation shell is large, the transferred charge is distributed over more molecules, resulting in smaller frequency changes, which are likely due to differences in the size of the first solvent shell since these molecules are most strongly coupled to the electron.[66] From this, we hypothesize that the ∼200 cm^{-1} downshift measured for e$^-$(H_2O) versus the 340 cm^{-1} for e$^-$(CH_3OH) reveals that an electron in liquid methanol is surrounded by significantly fewer solvent molecules in the first shell relative to an electron solvated in water. This general conclusion is consistent with the ESEEM experiments on frozen glasses, where it was concluded that there are six solvent molecules in the first shell of e$^-$(H_2O) versus four solvent molecules for e$^-$(MeOH).[7,9] This conclusion disagrees with MD simulations of electrons in water and methanol, which show equivalent coordination numbers in both solvents.[4,31] Furthermore, our conclusion is consistent with many experimental studies of halide solvation[29] as well as several MD simulations of halide ions, specifically bromide, which has a radius similar to that of the solvated electron in water.[4] The result from recent Car−Parrinello molecular dynamics simulations shows that Br$^-$ in methanol has a coordination number of four, whereas Br$^-$ in water has five or six molecules in the first shell.[67,68] Since all of the downshifts reported here for e$^-$(EtOH), e$^-$(*n*-PrOH), and e$^-$(*n*-BuOH) also exceed the downshifts for the hydrated electron, it is likely that the coordination number of these alcohols around the electron are likewise smaller.

The downshift of the librational mode by ∼120 cm^{-1} from a frequency of ∼650 cm^{-1} in the pure solvent reveals that the solvent molecules in the vicinity of the electron experience weaker tangential forces relative to molecules in the bulk solvent.[69] The weakened tangential forces have two origins. First, our data suggest that the solvent molecules in the first solvent shell have hydrogen bonds that are directed largely toward the electron, which would also imply that the H bonds between solvent molecules within this shell are disrupted. The loss of tangential restoring force in replacing a solvent−solvent hydrogen bond with an electron−solvent bond is reasonable, given the diffuse nature and low mass of the electron itself. Second, molecules in the first solvent shell are unable to donate a hydrogen bond to the second shell solvent molecules. Both factors reduce the tangential restoring forces on the molecules in the first solvent shell that likely contribute most to our RR intensities.

4.3. Resonance Raman Intensities. Our resonance Raman data also provide insights into the excited-state dynamics of this unique system. Time-dependent calculations utilizing both the experimentally determined resonance Raman cross sections and absorption spectra allow determination of the origin of the Franck−Condon coupling and the extent to which fast (homogeneous) and slow (inhomogeneous) mechanisms contribute to the solvent−solute dynamics.

The question of time scale for the fluctuations that broaden spectra in the condensed phase is a crucial one[70] and is particularly important in the case of solvated electrons in polar solvents, which exhibit remarkably broad absorption spectra. The full-width at half-maximum (fwhm) for solvated electrons in alcohols is ∼11000−13000 cm^{-1}, a factor of 1.6−1.9 times larger than the ∼6800 cm^{-1} fwhm of the hydrated electron.[49] The broad spectrum in alcohols is speculated to arise from a number of factors, including contributions from multiple electronic states,[31,49] large structural fluctuations for the electron−alcohol systems,[31,71] and coupling to intramolecular modes.[72,73] Our calculations (Table 2) indicate that, regardless of the choice of parameters that are ultimately selected, inhomogeneous broadening is dominant. This finding is bolstered by noting that the homogeneous broadening parameter that we found as an upper limit (1330 cm^{-1}) is likely artificially increased due to displacements along unseen (e.g., low-frequency librational or translational) modes that are below our spectral window. In these calculations, the dynamics that are considered inhomogeneous are ones that are slower than the ground-state vibrational dephasing time.[70] The greater contribution from inhomogeneous broadening for electron−alcohol systems contrasts with the results of a similar RR analysis for the hydrated electron,[13] where faster homogeneous dephasing processes play a relatively more important role than inhomogeneous broadening. Photon echo and hole-burning experiments agreed with the general picture from the Raman calculations of the hydrated electron.[24,74] Unfortunately similar ultrafast data are not available for comparison in the case of the electron−alcohol systems. MD simulations have also found significantly greater structural inhomogeneity and fluctuations for e^-(MeOH) relative to similar calculations on $e^-(H_2O)$[31] and may also be a possible reason for the broadened vibrational bands observed for e^-(MeOH) as compared to those of the pure solvent. Given the lack of any vibronic features in the absorption spectrum, additional ultrafast experiments, femtosecond hole-burning experiments, or perhaps simultaneous modeling of the RR and fluorescence emission[75] would be required to definitively select the best set of parameters among the various models listed in Table 2.

Our data shed light on the origin of the Franck−Condon displacements of the electron−alcohol systems. The enhanced normal modes include the CO stretch, CH_3 bend, CH_2 bend, COH bend, and the OH stretch. Surprisingly, the CH stretching bands that show the highest intensity for the pure solvent are not observable for the solvated electron. The selective enhancements of the modes arising from the alkyl portion of the alcohol, such as the CO stretch, CH_3 bend, and CH_2 bend, can be better understood by considering the internal (local) coordinates that comprise each normal mode. From the decomposition of each normal mode, we find that all enhanced RR modes of this study are either predominantly OH in character or have an A_{ji} of ∼1 or greater from the COH bend internal coordinate (A_{ji} is the matrix of normal mode vectors relating normal coordinates to internal basis coordinates). We conclude that the enhancement of select Raman modes, resulting from Franck−Condon coupling, is primarily mediated via the strong interaction of the OH group with the electron. Consistent with our findings, the unobserved CH stretching modes do not include significant contribution from OH motion.

Of all the observed modes, the libration shows the largest enhancement, indicating that it plays a significant role in the solvation dynamics immediately following s → p excitation of the electron. This is true regardless of the set of the parameters chosen from Table 2. The importance of librational motion is not an intuitive result because the excitation of the solvated electron does not cause a change in dipole moment, which is the typical perturbation that initiates the solvent reorientation in the vast majority of solvent−solute studies.[33,76] Early molecular dynamics simulations had therefore focused on the large change in "volume" of the solvated electron upon photoexcitation and stressed the importance of translational modes in the immediate solvent response for the hydrated electron.[26,77] The fact that we see strong librational enhancements for the solvated electron systems implies that these faster rotational motions are a critical part of the ultrafast response of the solvent. Apparently, the change in electron density requires that the solvent molecules rotate immediately in the Franck−Condon region. Since librations are quite effective at breaking the solute−solvent hydrogen bonds,[34] perhaps this motion facilitates the breaking of hydrogen bonds that existed in the ground state and commences the formation of new hydrogen bonds to stabilize the excited-state distribution. Consistent with this hypothesis, MD simulations probing the solvent response immediately following the excitation of the electron conclude that the H-bond structure in the first shell of the excited state is very different from the ground state and that significant rearrangement must occur upon photoexcitation.[31]

One apparent contradiction to our finding that the librations are significantly coupled to the electronic transition is that no isotope effect was observed in a transient absorption experiment with a time resolution of ∼150 fs.[37,78] We expect that an isotope effect of $\sqrt{2}$ will be found in ultrafast pump−probe and photon echo studies of the electron−alcohol systems, once sufficient time resolution (<50 fs) is employed.[12,38]

5. Conclusions

Our data provide the first structural information on the solvated electron in liquid alcohols and show that the resonance Raman spectra are due to Franck−Condon coupling of the electronic transition of the electron to the vibrations of nearby solvent molecules. We find no vibrational evidence for the formation of any new molecular species associated with the electron, and the strong correlation of the vibrational structure with that of the pure solvents shows that the electron acts only as a perturbation to the solvent structure. Frequency shifts of the libration also reveal that the hydrogen-bonding structure is disrupted in the presence of the electron. The downshifted OH stretch frequencies suggest that solvent molecules of e^-(MeOH) adopt a bond-oriented structure, while e^-(EtOH) and e^-(*n*-PrOH) adopt more of a dipole orientation. Additionally, the number of solvent molecules that are Franck−Condon coupled to the electron appears to be significantly fewer than the number of waters coupled to the aqueous solvated electron.

Resonance Raman intensity analysis also sheds light on the origin of the solute−solvent coupling, the extent to which homogeneous and inhomogeneous mechanisms contribute, and the importance of the librational mode in the solvent response upon electron excitation. The solvent bands found to couple to the electronic transition of the electron are those which have significant contribution from an internal OH coordinate. All sets

of parameters from the time-dependent calculations also highlight the importance of inhomogeneous mechanisms in the solute−solvent dynamics. Last, the librational motion is found to play a large role in the dynamics following photoexcitation. These conclusions provide an enhanced molecular view of the solvated electron and reveal new aspects about the solvation dynamics for solvated electrons in alcohols.

Acknowledgment. We thank Renee Frontiera for many helpful discussions and Kaiser Optical for loaning the 780 nm SuperPlus Notch filter. This work was supported by the Mathies Royalty Fund.

Supporting Information Available: Additional experimental and theoretical results. This material is available free of charge via the Internet at http://pubs.acs.org.

References and Notes

(1) Chandler, D. Electron Transfer in Water and Other Polar Environments, How It Happens. In *Classical and Quantum Dynamics in Condensed Phase Simulations*; Berne, B. J., Ciccotti, G., Coker, D. F., Eds.; World Scientific: Singapore, 1998; p 25.

(2) Zhou, Y. F.; Morais-Cabral, J. H.; Kaufman, A.; MacKinnon, R. *Nature* **2001**, *414*, 43.

(3) Sprik, M.; Impey, R. W.; Klein, M. L. *J. Chem. Phys.* **1985**, *83*, 5802.

(4) Rossky, P. J.; Schnitker, J. *J. Phys. Chem.* **1988**, *92*, 4277.

(5) Wallqvist, A.; Martyna, G.; Berne, B. J. *J. Phys. Chem.* **1988**, *92*, 1721.

(6) Deng, Z. H.; Martyna, G. J.; Klein, M. L. *Phys. Rev. Lett.* **1993**, *71*, 267.

(7) Schlick, S.; Narayana, P. A.; Kevan, L. *J. Chem. Phys.* **1976**, *64*, 3153.

(8) Ichikawa, T.; Kevan, L.; Bowman, M. K.; Dikanov, S. A.; Tsvetkov, Y. D. *J. Chem. Phys.* **1979**, *71*, 1167.

(9) Kevan, L. *Chem. Phys. Lett.* **1979**, *66*, 578.

(10) Narayana, M.; Kevan, L. *J. Chem. Phys.* **1980**, *72*, 2891.

(11) Mizuno, M.; Tahara, T. *J. Phys. Chem. A* **2001**, *105*, 8823.

(12) Tauber, M. J.; Mathies, R. A. *J. Phys. Chem. A* **2001**, *105*, 10952.

(13) Tauber, M. J.; Mathies, R. A. *Chem. Phys. Lett.* **2002**, *354*, 518.

(14) Mizuno, M.; Tahara, T. *J. Phys. Chem. A* **2003**, *107*, 2411.

(15) Tauber, M. J.; Mathies, R. A. *J. Am. Chem. Soc.* **2003**, *125*, 1394.

(16) Mizuno, M.; Yamaguchi, S.; Tahara, T. *J. Phys. Chem. A* **2005**, *109*, 5257.

(17) Tuttle, T. R.; Golden, S. *J. Phys. Chem.* **1991**, *95*, 5725.

(18) Shkrob, I. A. *J. Phys. Chem. A* **2006**, *110*, 3967.

(19) Hameka, H. F.; Robinson, G. W.; Marsden, C. J. *J. Phys. Chem.* **1987**, *91*, 3150.

(20) Neumann, S.; Eisfeld, W.; Sobolewski, A.; Domcke, W. *Phys. Chem. Chem. Phys.* **2004**, *6*, 5297.

(21) Neumann, S.; Eisfeld, W.; Sobolewski, A. L.; Domcke, W. *J. Phys. Chem. A* **2006**, *110*, 5613.

(22) Shi, X. L.; Long, F. H.; Lu, H.; Eisenthal, K. B. *J. Phys. Chem.* **1996**, *100*, 11903.

(23) Yokoyama, K.; Silva, C.; Son, D. H.; Walhout, P. K.; Barbara, P. F. *J. Phys. Chem. A* **1998**, *102*, 6957.

(24) Baltuska, A.; Emde, M. F.; Pshenichnikov, M. S.; Wiersma, D. A. *J. Phys. Chem. A* **1999**, *103*, 10065.

(25) Bratos, S.; Leicknam, J. C.; Borgis, D.; Staib, A. *Phys. Rev. E* **1997**, *55*, 7217.

(26) Mosyak, A. A.; Prezhdo, O. V.; Rossky, P. J. *J. Chem. Phys.* **1998**, *109*, 6390.

(27) Minary, P.; Turi, L.; Rossky, P. J. *J. Chem. Phys.* **1999**, *110*, 10953.

(28) Bedard-Hearn, M. J.; Larsen, R. E.; Schwartz, B. J. *Phys. Rev. Lett.* **2006**, *97*.

(29) Ohtaki, H.; Radnai, T. *Chem. Rev.* **1993**, *93*, 1157.

(30) Shkrob, I. A. E-Prints in Physics, Mathematics, Computer Science and Quantitative Biology. http://arxiv.org/pdf/physics/0607228.

(31) Turi, L.; Mosyak, A.; Rossky, P. J. *J. Chem. Phys.* **1997**, *107*, 1970.

(32) Turi, L. *J. Chem. Phys.* **1999**, *110*, 10364.

(33) Maroncelli, M.; Macinnis, J.; Fleming, G. R. *Science* **1989**, *243*, 1674.

(34) Fonseca, T.; Ladanyi, B. M. *J. Mol. Liq.* **1994**, *60*, 1.

(35) Barthel, J.; Bachhuber, K.; Buchner, R.; Hetzenauer, H. *Chem. Phys. Lett.* **1990**, *165*, 369.

(36) Kenney-Wallace, G. A. *Acc. Chem. Res.* **1978**, *11*, 433.

(37) Silva, C.; Walhout, P. K.; Reid, P. J.; Barbara, P. F. *J. Phys. Chem. A* **1998**, *102*, 5701.

(38) Silva, C.; Walhout, P. K.; Yokoyama, K.; Barbara, P. F. *Phys. Rev. Lett.* **1998**, *80*, 1086.

(39) Borgis, D.; Rossky, P. J.; Turi, L. *J. Chem. Phys.* **2006**, *125*, 064501

(40) Tauber, M. J.; Stuart, C. M.; Mathies, R. A. *J. Am. Chem. Soc.* **2004**, *126*, 3414.

(41) Myers, A. B.; Mathies, R. A. Resonance Raman Intensities: A Probe of Excited-State Structure and Dynamics. In *Biological Applications of Raman Spectroscopy: Resonance Raman Spectra of Polyenes and Aromatics*; Spiro, T. G., Ed.; John Wiley & Sons: New York, 1987; Vol. 2, p 1.

(42) Vilchiz, V. H.; Chen, X. Y.; Kloepfer, J. A.; Bradforth, S. E. *Radiat. Phys. Chem.* **2005**, *72*, 159.

(43) Buxton, G. V.; Greenstock, C. L.; Helman, W. P.; Ross, A. B. *J. Phys. Chem. Ref. Data* **1988**, *17*, 513.

(44) Tauber, M. J.; Mathies, R. A.; Chen, X. Y.; Bradforth, S. E. *Rev. Sci. Instrum.* **2003**, *74*, 4958.

(45) Sauer, M. C.; Arai, S.; Dorfman, L. M. *J. Chem. Phys.* **1965**, *42*, 708.

(46) Jou, F. Y.; Freeman, G. R. *J. Phys. Chem.* **1977**, *81*, 909.

(47) Herrmann, V.; Krebs, P. *J. Phys. Chem.* **1995**, *99*, 6794.

(48) Colles, M. J.; Griffiths, J. E. *J. Chem. Phys.* **1972**, *56*, 3384.

(49) Jou, F. Y.; Freeman, G. R. *Can. J. Chem.* **1979**, *57*, 591.

(50) Tuttle, T. R.; Golden, S.; Rosenfeld, G. *Radiat. Phys. Chem.* **1988**, *32*, 525.

(51) Frisch, M. J.; Trucks, G. W.; Schlegel, H. B.; Scuseria, G. E.; Robb, M. A.; Cheeseman, J. R.; Montgomery, J. A., Jr.; Vreven, T.; Kudin, K. N.; Burant, J. C.; Millam, J. M.; Iyengar, S. S.; Tomasi, J.; Barone, V.; Mennucci, B.; Cossi, M.; Scalmani, G.; Rega, N.; Petersson, G. A.; Nakatsuji, H.; Hada, M.; Ehara, M.; Toyota, K.; Fukuda, R.; Hasegawa, J.; Ishida, M.; Nakajima, T.; Honda, Y.; Kitao, O.; Nakai, H.; Klene, M.; Li, X.; Knox, J. E.; Hratchian, H. P.; Cross, J. B.; Bakken, V.; Adamo, C.; Jaramillo, J.; Gomperts, R.; Stratmann, R. E.; Yazyev, O.; Austin, A. J.; Cammi, R.; Pomelli, C.; Ochterski, J. W.; Ayala, P. Y.; Morokuma, K.; Voth, G. A.; Salvador, P.; Dannenberg, J. J.; Zakrzewski, V. G.; Dapprich, S.; Daniels, A. D.; Strain, M. C.; Farkas, O.; Malick, D. K.; Rabuck, A. D.; Raghavachari, K.; Foresman, J. B.; Ortiz, J. V.; Cui, Q.; Baboul, A. G.; Clifford, S.; Cioslowski, J.; Stefanov, B. B.; Liu, G.; Liashenko, A.; Piskorz, P.; Komaromi, I.; Martin, R. L.; Fox, D. J.; Keith, T.; Al-Laham, M. A.; Peng, C. Y.; Nanayakkara, A.; Challacombe, M.; Gill, P. M. W.; Johnson, B.; Chen, W.; Wong, M. W.; Gonzalez, C.; Pople, J. A. *Gaussian 03*; Gaussian, Inc.: Wallingford, CT, 2004.

(52) Bertie, J. E.; Zhang, S. L. *J. Chem. Phys.* **1994**, *101*, 8364.

(53) Falk, M.; Whalley, E. *J. Chem. Phys.* **1961**, *34*, 1554.

(54) Florian, J.; Leszczynski, J.; Johnson, B. G.; Goodman, L. *Mol. Phys.* **1997**, *91*, 439.

(55) Bartels, D. M.; Takahashi, K.; Cline, J. A.; Marin, T. W.; Jonah, C. D. *J. Phys. Chem. A* **2005**, *109*, 1299.

(56) Kim, J.; Lee, H. M.; Suh, S. B.; Majumdar, D.; Kim, K. S. *J. Chem. Phys.* **2000**, *113*, 5259.

(57) Corbett, C. A.; Martinez, T. J.; Lisy, J. M. *J. Phys. Chem. A* **2002**, *106*, 10015.

(58) Robertson, W. H.; Karapetian, K.; Ayotte, P.; Jordan, K. D.; Johnson, M. A. *J. Chem. Phys.* **2002**, *116*, 4853.

(59) Hester, R. E.; Plane, R. A. *Spectrochim. Acta, Part A* **1967**, *23*, 2289.

(60) Hidaka, F.; Yoshimura, Y.; Kanno, H. *J. Solution Chem.* **2003**, *32*, 239.

(61) Schultz, J. W.; Hornig, D. F. *J. Phys. Chem.* **1961**, *65*, 2131.

(62) Weston, R. E. *Spectrochim. Acta* **1962**, *18*, 1257.

(63) Kammrath, A., Verlet, J. R. R.; Griffin, G. B.; Neumark, D. M. *J. Chem. Phys.* **2006**, *125*, 171102.

(64) Bublitz, G. U.; Boxer, S. G. *Annu. Rev. Phys. Chem.* **1997**, *48*, 213.

(65) Thompson, W. H.; Hynes, J. T. *J. Am. Chem. Soc.* **2000**, *122*, 6278.

(66) Mosyak, A. A.; Prezhdo, O. V.; Rossky, P. J. *J. Mol. Struct.* **1999**, *486*, 545.

(67) Raugei, S.; Klein, M. L. *J. Am. Chem. Soc.* **2001**, *123*, 9484.

(68) Faralli, C.; Pagliai, M.; Cardini, G.; Schettino, V. *J. Phys. Chem. B* **2006**, *110*, 14923.

(69) Although methanol possesses three librations, only the OH libration about the CO axis is considered to contribute significantly to the dynamics and will be considered for discussion.[66]

(70) Myers, A. B. *Annu. Rev. Phys. Chem.* **1998**, *49*, 267.

(71) Carmichael, I. *J. Phys. Chem.* **1980**, *84*, 1076.

(72) Banerjee, A.; Simons, J. *J. Chem. Phys.* **1978**, *68*, 415.

(73) Abramczyk, H.; Kroh, J. *J. Phys. Chem.* **1991**, *95*, 5749.

(74) Cavanagh, M. C.; Martini, I. B.; Schwartz, B. J. *Chem. Phys. Lett.* **2004**, *396*, 359.

(75) Li, B. J.; Alan, E.; Mukamel, S.; Myers, A. B. *J. Am. Chem. Soc.* **1994**, *116*, 11039.

(76) Bardeen, C. J.; Rosenthal, S. J.; Shank, C. V. *J. Phys. Chem. A* **1999**, *103*, 10506.

(77) Schwartz, B. J.; Rossky, P. J. *J. Chem. Phys.* **1996**, *105*, 6997.

(78) Shi, X. L.; Long, F. H.; Lu, H.; Eisenthal, K. B. *J. Phys. Chem.* **1995**, *99*, 6917.